NUMERICAL SOLUTION OF A NONLINEAR EIGENVALUE PROBLEM ARISING IN OPTIMAL INSULATION

SÖREN BARTELS AND GIUSEPPE BUTTAZZO

Abstract. The optimal insulation of a heat conducting body by a thin film of variable thickness can be formulated as a nondifferentiable, nonlocal eigenvalue problem. The discretization and iterative solution for the reliable computation of corresponding eigenfunctions that determine the optimal layer thickness are addressed. Corresponding numerical experiments confirm the theoretical observation that a symmetry breaking occurs for the case of small available insulation masses and provide insight in the geometry of optimal films. An experimental shape optimization indicates that convex bodies with one axis of symmetry have favorable insulation properties.

1. Introduction

Improving the mechanical properties of an elastic body by surrounding it by a thin reinforcing film of a different material is a classical and well understood problem in mathematical analysis [BCF80, Fri80, AB86, CKU99]. A recent result in [BBN17] proves the surprising fact that in the case of a small amount of material for the surrounding layer, an unexpected break of symmetry occurs, i.e., a nonuniform arrangement on the surface of a ball leads to better material properties than a uniform one.

The case of the heat equation is similar, and a model reduction for thin films leads, in the long-time behavior, to a partial differential equation with Robin type boundary condition, e.g.,

$$-\Delta u = f \text{ in } \Omega, \qquad \ell\,\partial_n u + u = 0 \text{ on } \partial\Omega,$$

i.e., the heat flux $-\partial_n u$ trough the boundary is given by the temperature difference divided by the scaled nonnegative layer thickness ℓ. A vanishing tickness thus leads to a homogenous Dirichlet boundary condition which prescribes the external temperature (set to zero), while as $\ell \to +\infty$ the boundary condition above approaches the Neumann one, corresponding to a perfect insulation. The long-time insulation properties (decay rate of the

Date: August 12, 2017.

1991 *Mathematics Subject Classification.* 35J25,49R05,65N12,65N25.

Key words and phrases. optimal insulation, symmetry breaking, numerical scheme.

temperature) are determined by the principal eigenvalue of the corresponding differential operator, i.e.,

$$\lambda_\ell = \inf\left\{\int_\Omega |\nabla u|^2\,\mathrm{d}x + \int_{\partial\Omega} \ell^{-1}u^2\,\mathrm{d}s \;:\; \int_\Omega u^2\,\mathrm{d}x = 1\right\}$$

The optimality of the layer is characterized by minimality of λ_ℓ among admissible arrangements $\ell : \partial\Omega \to \mathbb{R}_+$ with prescribed total mass m, i.e., $\|\ell\|_{L^1(\partial\Omega)} = m$. Interchanging the minimization with respect to ℓ and u leads to an explicit formula for the optimal ℓ, through the nonlinear eigenvalue problem

$$\begin{aligned}\lambda_m &= \inf\left\{\lambda_\ell \;:\; \int_{\partial\Omega} \ell\,\mathrm{d}s = m\right\}\\ &= \inf\left\{\int_\Omega |\nabla u|^2\,\mathrm{d}x + \frac{1}{m}\Big(\int_{\partial\Omega}|u|\,\mathrm{d}s\Big)^2 \;:\; \int_\Omega u^2\,\mathrm{d}x = 1\right\}.\end{aligned}$$

The calculation shows that optimal layers ℓ are proportional to traces of nonnegative eigenfunctions u_m on $\partial\Omega$.

The results in [BBN17] prove in a nonconstructive way that for the unit ball nonradial eigenfunctions exist if and only if $0 < m < m_0$, where m_0 is a critical mass corresponding to the first nontrivial Neumann eigenvalue of the Laplace operator. In particular, the symmetry breaking occurs if and only if $\lambda_N < \lambda_m < \lambda_D$, where λ_N and λ_D denote the first (nontrivial) eigenvalues of the Laplacian with Neumann and Dirichlet boundary conditions.

While the proof of the result above implies that optimal nonradial insulating films have to leave gaps (i.e. regions on $\partial\Omega$ where $\ell = 0$) on the surface of the ball, the analysis does not characterize further properties such as symmetry or connectedness of the gaps. It is therefore desirable to gain insight of qualitative and quantitative features via accurate numerical simulations.

Computing solutions for the nonlinear eigenvalue problem defining λ_m is a challenging task since this requires solving a nondifferentiable, nonlocal, constrained minimization problem. To cope with these difficulties we adopt a gradient flow approach of a suitable regularization of the minimization problem, i.e., we consider the evolution problem

$$(\partial_t u, v) + (\nabla u, \nabla v) + \frac{1}{m}\Big(\int_{\partial\Omega} |u|_\varepsilon\,\mathrm{d}s\Big)\int_{\partial\Omega}\frac{uv}{|u|_\varepsilon}\,\mathrm{d}s = 0.$$

Here, $(\cdot,\cdot)$ denotes the L^2 inner product on Ω. The regularized modulus is defined via $|a|_\varepsilon = (a^2+\varepsilon^2)^{1/2}$ and the constraint $\|u\|_{L^2} = 1$ is incorporated via the conditions

$$(\partial_t u, u) = 0, \qquad (v, u) = 0.$$

With the backward difference quotient $d_t u^k = (u^k - u^{k-1})/\tau$ for a step size $\tau > 0$ we consider a semi-implicit discretization defined by the sequence of problems that determines the sequence $(u^k)_{k=0,1,\dots}$ for a given initial u^0

recursively via

$$(d_t u^k, v) + (\nabla u^k, \nabla v) + m^{-1}\Big(\int_{\partial\Omega} |u^{k-1}|_\varepsilon \,\mathrm{d}s\Big)\int_{\partial\Omega} \frac{u^k v}{|u^{k-1}|_\varepsilon}\,\mathrm{d}s = 0,$$

for all test functions v subject to the constraints

$$(d_t u^k, u^{k-1}) = 0, \qquad (v, u^{k-1}) = 0.$$

Note that every step only requires the solution of a constrained linear elliptic problem. Crucial for this is the semi-implicit treatment of the nondifferentiable and nonlocal boundary term and the normalization constraint. We show that this time-stepping scheme is nearly unconditionally energy decreasing in terms of τ and ε and that the constraint is approximated appropriately. The stability analysis is related to estimates for numerical schemes for mean curvature and total variation flows investigated in [Dzi99, BDN17]. The spatial discretization of the minimization problem and the iterative scheme require an appropriate numerical integration of the boundary terms. We provide a full error analysis for the use of a straightforward trapezoidal rule avoiding unjustified regularity assumptions. This leads to a convergence rate for the approximation of λ_m incorporating both the mesh size $h > 0$ and the regularization parameter $\varepsilon > 0$. The good stability properties of the discrete gradient flow and the accuracy of the spatial discretization are illustrated by means of numerical experiments. These reveal that for moderate triangulations with a few thousand elements a small number of iterations is sufficient to capture the characteristic properties of solutions of the nonlinear eigenvalue problem and thereby gain understanding in the features of optimal nonsymmetric insulating films for the unit ball in two and three space dimensions.

We also investigate the idea of improving the insulation properties by modifying the shape of a heat conducting body. In the case of two space dimensions we use a shape derivative and deform a given domain via a negative shape gradient obtained via appropriate Stokes problems. Corresponding numerical experiments confirm the observation from [BBN17] that the disk is not optimal when the total amount m of insulating material is small and that instead convex domains with one axis of symmetry lead to smaller principal eigenvalues.

In three or more space dimensions the situation is more complex: indeed an optimal shape does not exist. In fact, if Ω is composed of a large number n of small disjoint balls of radius $r_n \to 0$ we may define

$$u = \begin{cases} 1 & \text{on one of the balls} \\ 0 & \text{on the remaining ones} \end{cases}$$

and we obtain, if B is the ball where $u = 1$,

$$\lambda_m(\Omega) \le \frac{\frac{1}{m}(|\partial B|)^2}{|B|} = \frac{d^2\omega_d}{m} r_n^{d-2}\,,$$

where ω_d denotes the Lebesgue measure of the unit ball in $\mathbb{R}^d$. If $d \geq 3$ we then obtain that $\lambda_m(\Omega)$ may be arbitrarily close to zero. Nevertheless, starting with a ball as the initial domain and performing a shape variation among rotational bodies, we numerically identify ellipsoids and egg-shaped domains that have good insulation properties.

In spite of the nonexistence argument above, it is desirable to prove (or disprove) that an optimal domain exists in a restricted class, as for instance the class of convex domains. The numerical experiments of Section 6 indicate that convex bodies are optimal among rotational bodies, which is a good sign for the existence of an optimal body among convex ones.

The article is organized as follows. In Section 2 we outline the derivation of the nonlinear eigenvalue problem. In Section 3 we investigate the stability properties of the semi-implicit discretization of the gradient flow used as an iterative scheme for computing eigenfunctions. Section 4 is devoted to the analysis of the spatial discretization of the problem. Experiments confirming the stability and approximation properties and revealing the qualitative and quantitative properties of optimal insulating films are presented in Section 5. In Section 6 we experimentally investigate the numerical optimization of the shape of insulated conducting bodies.

2. Nonlinear eigenvalue problem

We consider a heat conducting body $\Omega \subset \mathbb{R}^d$ that is surrounded by an insulating material of variable normal thickness $\varepsilon\ell \geq 0$, cf. Fig. 1. A model reduction for vanishing conductivity $\varepsilon \to 0$ in the insulating layer leads, for the stationary temperature u under the action of heat sources f, to an elliptic partial differential equation, with Robin type boundary condition, i.e.,

$$-\Delta u = f \text{ in } \Omega, \qquad \ell\,\partial_n u + u = 0 \text{ on } \partial\Omega,$$

cf. [BCF80, AB86] for details. The boundary condition states that the heat flux through the boundary is given by the temperature difference divided by thickness of the insulating material.

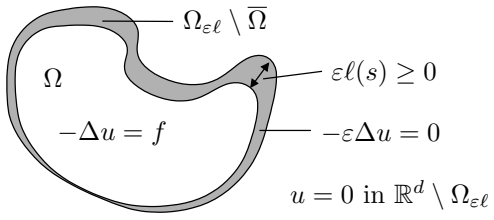

Figure 1. Conducting body surrounded by insulating material of variable normal thickness $\varepsilon\ell \geq 0$.

It has to be noticed that the only interesting case occurs when the conductivity and the thickness of the insulating material have the same order of magnitude. Indeed, if conductivity is significantly smaller than thickness

the limit problem is the Neumann one, while in the converse situation one obtains the Dirichlet problem.
The optimization of the thickness of the thin insulating layer, once the total amount of insulator $\|\ell\|_{L^1}$ is prescribed, is illustrated in [BBN17]. Here we deal with the case when no heat source is present, so that the temperature u, starting from its initial datum, tends to zero as $t \to +\infty$. It is well known that the temperature decays exponentially in time at a rate given by the first eigenvalue λ_ℓ of the differential operator $\mathcal{A}_\ell$ defined by

$$\langle \mathcal{A}_\ell u, v\rangle = \int_\Omega \nabla u \cdot \nabla v \, \mathrm{d}x + \int_{\partial\Omega} \ell^{-1} uv \, \mathrm{d}s, \qquad u, v \in H^1(\Omega).$$

We have then

$$\lambda_\ell = \min\left\{ \langle \mathcal{A}_\ell u, u\rangle \ : \ \int_\Omega |u|^2 \, \mathrm{d}x = 1 \right\}$$

and, if we look for the distribution of insulator around Ω which gives the slowest decay in time, we have to solve the optimization problem

$$\min\left\{ \lambda_\ell \ : \ \int_{\partial\Omega} \ell \, \mathrm{d}s = m \right\},$$

where m represents the total amount of insulator at our disposal.
Since λ_ℓ is given by a minimum too, we may interchange the minima over ℓ and u obtaining that for a given $u \in H^1(\Omega)$ the optimal ℓ is such that u^2/ℓ^2 is constant on $\partial\Omega$ and hence given by

$$\ell(z) = \frac{m|u(z)|}{\int_{\partial\Omega} |u| \, \mathrm{d}s} \qquad \text{for } z \in \partial\Omega.$$

An optimal thickness ℓ is thus directly obtained from a solution of the nonlinear eigenvalue problem

$$\lambda_m = \min\left\{ J_m(u) \ : \ \int_\Omega |u|^2 \, \mathrm{d}x = 1 \right\}$$

where J_m is the functional defined on $H^1(\Omega)$ by

$$J_m(u) = \int_\Omega |\nabla u|^2 \, \mathrm{d}x + \frac{1}{m}\Big(\int_{\partial\Omega} |u| \, \mathrm{d}s \Big)^2.$$

The mapping $m \mapsto \lambda_m$ is a continuous and strictly decreasing function with the asymptotic values

$$\lim_{m\to 0} \lambda_m = \lambda_D, \qquad \lim_{m\to\infty} \lambda_m = 0,$$

which represent the first Dirichlet and Neumann eigenvalues of the Laplacian.
When Ω is a ball, denoting by

$$\lambda_N = \min\left\{ \int_\Omega |\nabla u|^2 \, \mathrm{d}x \ : \ \int_\Omega u^2 \, \mathrm{d}x = 1, \ \int_\Omega u \, \mathrm{d}x = 0 \right\}$$

the first nontrivial Neumann eigenvalue, we have $0 < \lambda_N < \lambda_D$ and there exists $m_0 > 0$ such that (cf. Fig. 2) $\lambda_{m_0} = \lambda_N$.

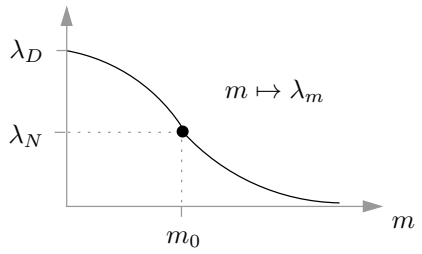

FIGURE 2. Dependence of the principal eigenvalue λ_m of $\mathcal{A}_\ell$ on available mass $m > 0$ in the case of a ball.

We summarize below the main result concerning this break of symmetry and refer to [BBN17] for details.

Theorem 2.1 ([BBN17])**.** *Let Ω be a ball. If $m > m_0$ every solution u_m of the minimization problem defining λ_m is radial, hence the optimal thickness ℓ of the insulating film around Ω is constant. On the contrary, if $0 < m < m_0$ the solution u_m is not radial and so the optimal thickness ℓ is not constant.*

The proof of the theorem also shows that nonuniform optimal insulations ℓ leave gaps, i.e., the support of an optimal ℓ is a strict subset of $\partial\Omega$.

3. Iterative minimization

We aim at iteratively minimizing the regularized functional

$$J_{m,\varepsilon}(u) = \|\nabla u\|^2 + \frac{1}{m}\|u\|^2_{L^1_\varepsilon(\partial\Omega)}$$

among functions $u \in H^1(\Omega)$ with $\|u\|^2 = 1$ and with the regularized L^1 norm defined via the regularized modulus

$$|a|_\varepsilon = (a^2 + \varepsilon^2)^{1/2}.$$

Minimizers satisfy the eigenvalue equation

$$(\nabla u, \nabla v) + \frac{1}{m}\|u\|_{L^1_\varepsilon(\partial\Omega)} \int_{\partial\Omega} \frac{uv}{|u|_\varepsilon}\,\mathrm{d}s = \lambda_m(u, v)$$

for all $v \in H^1(\Omega)$. To define an iterative scheme we consider the corresponding evolution problem which seeks for given $u_0 \in H^1(\Omega)$ a family $u : [0, T] \to H^1(\Omega)$ with $u(0) = u_0$, $\|u(t)\|^2 = 1$ for all $t \in [0, T]$, and

$$(\partial_t u, v)_* + (\nabla u, \nabla v) + \frac{1}{m}\|u\|_{L^1_\varepsilon(\partial\Omega)} \int_{\partial\Omega} \frac{uv}{|u|_\varepsilon}\,\mathrm{d}s = \lambda_m(u, v)$$

for all $t \in (0, T]$ and $v \in H^1(\Omega)$. Here, $(\cdot, \cdot)_*$ is an appropriate inner product defined on $H^1(\Omega)$. Noting that $(\partial_t u, u) = 0$ it suffices to restrict to test functions $v \in H^1(\Omega)$ with $(u, v) = 0$ so that the right-hand side with the unknown multiplier λ_m disappears. Replacing the time derivative by a backward difference quotient and discretizing the nonlinear boundary term

and the constraint $(\partial_t u, u) = 0$ semi-implicitly to obtain linear problems in the time steps leads to the following numerical scheme.

Algorithm 3.1. *Let $\varepsilon, \tau > 0$ and $u_0 \in H^1(\Omega)$ with $\|u_0\|^2 = 1$; set $k = 1$.*
(1) Compute $u^k \in H^1(\Omega)$ such that $(d_t u^k, u^{k-1}) = 0$ and

$$(d_t u^k, v)_* + (\nabla u^k, \nabla v) + \frac{1}{m}\|u^{k-1}\|_{L^1_\varepsilon(\partial\Omega)} \int_{\partial\Omega} \frac{u^k v}{|u^{k-1}|_\varepsilon} \,\mathrm{d}s = 0$$

for all $v \in H^1(\Omega)$ with $(v, u^{k-1}) = 0$.
(2) Stop if $\|d_t u^k\|_* \le \varepsilon_{\mathrm{stop}}$; increase $k \to k+1$ and continue with (1) otherwise.

The iterates of Algorithm 3.1 approximate the continuous evolution equation and satisfy an approximate energy estimate on finite intervals $[0, T]$.

Proposition 3.2. *Assume that the induced norm $\|\cdot\|_*$ on $H^1(\Omega)$ is such that we have the trace inequality*

$$(1+\varepsilon)\|v\|^2_{L^1(\partial\Omega)} \le c^2_{\mathrm{Tr}}\|v\|^2_* + \|\nabla v\|^2$$

for some constant $c_{\mathrm{Tr}} > 0$ and all $v \in H^1(\Omega)$. Then Algorithm 3.1 is energy-decreasing in the sense that for every $K = 0, 1, \dots, \lfloor T/\tau \rfloor$ we have

$$J_{m,\varepsilon}(u^K) + 2\Big(1 - \frac{c^2_{\mathrm{Tr}}\tau}{2m}\Big)\tau \sum_{k=1}^{K} \|d_t u^k\|^2_* \le J_{m,\varepsilon}(u^0) + \frac{\varepsilon}{m} T(1+\varepsilon)|\partial\Omega|^2.$$

Moreover, if $\|u^0\|^2 = 1$ we have that

$$\|u^K\|^2 = 1 + \tau^2 \sum_{k=1}^{K} \|d_t u^k\|^2,$$

i.e., $\|u^K\| \ge 1$ and if $\|v\| \le c_*\|v\|_*$ for all $v \in H^1(\Omega)$ then $\big|\|u^K\|^2 - 1\big| \le c_{\mathrm{U}}\tau$.

Proof. Choosing $v = d_t u^k$ in Step (1) of Algorithm 3.1 shows that

$$\begin{aligned}\|d_t u^k\|^2_* + \frac{1}{2} d_t \|\nabla u^k\|^2 + \frac{\tau}{2}\|\nabla d_t u^k\|^2 \\ + \frac{1}{m}\|u^{k-1}\|_{L^1_\varepsilon(\partial\Omega)} \int_{\partial\Omega} \frac{(1/2)\big(d_t|u^k|^2 + \tau|d_t u^k|^2\big)}{|u^{k-1}|_\varepsilon} \,\mathrm{d}s = 0.\end{aligned}$$

We expect the last term on the left-hand side to be related to a discrete time derivative of the square of the regularized L^1 norm on the boundary. To verify this, we note that we have

$$d_t|u^k|_\varepsilon = d_t \frac{|u^k|^2_\varepsilon}{|u^k|_\varepsilon} = \frac{d_t|u^k|^2_\varepsilon}{|u^{k-1}|_\varepsilon} - \frac{|u^k|_\varepsilon d_t|u^k|_\varepsilon}{|u^{k-1}|_\varepsilon} = \frac{(1/2)\big(d_t|u^k|^2_\varepsilon - \tau|d_t|u^k|_\varepsilon|^2\big)}{|u^{k-1}|_\varepsilon}.$$

Using that $d_t|u^k|_\varepsilon^2 = d_t|u^k|^2$ we combine the two identities to verify that

$$\|d_t u^k\|_*^2 + \frac{1}{2} d_t \|\nabla u^k\|^2 + \frac{\tau}{2}\|\nabla d_t u^k\|^2 + \frac{1}{m}\|u^{k-1}\|_{L^1_\varepsilon(\partial\Omega)} d_t \|u^k\|_{L^1_\varepsilon(\partial\Omega)} + \frac{\tau}{2m}\|u^{k-1}\|_{L^1_\varepsilon(\partial\Omega)} \int_{\partial\Omega} \frac{|d_t|u^k|_\varepsilon|^2 + |d_t u^k|^2}{|u^{k-1}|_\varepsilon}\,\mathrm{d}s = 0.$$

Note that the last term on the left-hand side is non-negative. We use that

$$\|u^{k-1}\|_{L^1_\varepsilon(\partial\Omega)} d_t \|u^k\|_{L^1_\varepsilon(\partial\Omega)} = \frac{1}{2} d_t \|u^k\|^2_{L^1_\varepsilon(\partial\Omega)} - \frac{\tau}{2}\|d_t u^k\|^2_{L^1_\varepsilon(\partial\Omega)}$$

to deduce

$$\begin{aligned}\|d_t u^k\|_*^2 + \frac{1}{2} d_t\big(\|\nabla u^k\|^2 + \frac{1}{m}\|u^k\|^2_{L^1_\varepsilon(\partial\Omega)}\big) + \frac{\tau}{2}\|\nabla d_t u^k\|^2 &\le \frac{\tau}{2m}\|d_t u^k\|^2_{L^1_\varepsilon(\partial\Omega)} \\ &\le (1+\varepsilon)\frac{\tau}{2m}\|d_t u^k\|^2_{L^1(\partial\Omega)} + \frac{\tau}{2m}\big(\varepsilon+\varepsilon^2\big)|\partial\Omega|^2.\end{aligned}$$

The condition that

$$(1+\varepsilon)\|v\|^2_{L^1(\partial\Omega)} \le c_{\mathrm{Tr}}^2\|v\|_*^2 + \|\nabla v\|^2$$

and a summation over $k = 1, 2, \dots, K$ imply the stability estimate. We further note that due to the orthogonality $(d_t u^k, u^k) = 0$ we have

$$\|u^k\|^2 = \|u^{k-1}\|^2 + \tau^2\|d_t u^k\|^2$$

and an inductive argument yields the second asserted estimate. □

Remarks 3.3. *(i) If $\|\cdot\|_*$ is the norm in $H^1(\Omega)$ then the continuity of the trace operator implies the assumption. In case of the L^2 norm it depends on the geometry of Ω via the operator norm of the trace operator.*
(ii) The iterates of Algorithm 3.1 approximate an eigenfunction and since the values of J_m are (nearly) decreasing we expect to approximate λ_m since other eigenvalues correspond to unstable stationary configurations.
(iii) Since $\|u^K\| \ge 1$ we may normalize u^K and obtain an approximation of λ_m via $J_m(\widetilde{u}^K)$ with $\widetilde{u}^K = u^K/\|u^K\|$ even if $\tau = \mathcal{O}(1)$.

4. Spatial discretization

Given a regular triangulation $\mathcal{T}_h$ of Ω with maximal mesh-size $h > 0$ we consider the minimization of $J_{m,\varepsilon}$ in the finite element space

$$\mathcal{S}^1(\mathcal{T}_h) = \big\{v_h \in C(\overline{\Omega}) : v_h|_T \in P_1(T) \text{ for all } T \in \mathcal{T}_h\big\}.$$

For a direct implementability we include quadrature by considering the functional

$$J_{m,\varepsilon,h}(u_h) = \|\nabla u_h\|^2 + \frac{1}{m}\|u_h\|^2_{L^1_{\varepsilon,h}(\partial\Omega)}$$

with the discretized and regularized L^1 norm

$$\|u_h\|_{L^1_{\varepsilon,h}(\partial\Omega)} = \int_{\partial\Omega} \mathcal{I}_h|u_h|_\varepsilon\,\mathrm{d}s = \sum_{z\in\mathcal{N}_h\cap\partial\Omega} \beta_z|u_h(z)|_\varepsilon.$$

Here, $\mathcal{I}_h : C(\overline{\Omega}) \to \mathcal{S}^1(\mathcal{T}_h)$ is the nodal interpolation operator and $\mathcal{N}_h$ is the set of nodes in $\mathcal{T}_h$ so that we have

$$\beta_z = \int_{\partial\Omega} \varphi_z \, \mathrm{d}s$$

for the nodal basis function φ_z associated with $z \in \mathcal{N}_h$. It is a straightforward task to show that the result of Proposition 3.2 carries over to the spatially discretized functional $J_{m,\varepsilon,h}$. The following proposition determines the approximation properties of the discretized functional.

Proposition 4.1. *Assume that there exists a minimizer $u \in H^2(\Omega)$ for J_m with $\|u\|^2 = 1$. We then have*

$$0 \leq \min_{u_h \in \mathcal{S}^1(\mathcal{T}_h)} J_m(u_h) - J_m(u) \leq ch\|u\|^2_{H^2(\Omega)}.$$

Moreover, if $\mathcal{T}_h$ is quasiuniform then for every $u_h \in \mathcal{S}^1(\mathcal{T}_h)$ we have with $\alpha \geq 1/2$

$$\big|J_{m,\varepsilon,h}(u_h) - J_m(u_h)\big| \leq c(\|u_h\|_{H^1(\Omega)} + 1)^2(\varepsilon + h^\alpha).$$

If u_h is uniformly H^1-regular on the boundary, i.e., if $\|\nabla u_h\|_{L^2(\partial\Omega)} \leq c$ for all $h > 0$, then we have $\alpha \geq 1$.

Proof. (i) We define $\widetilde{u}_h = \mathcal{I}_h u / \|\mathcal{I}_h u\|$ which is well defined for h sufficiently small since $\|u - \mathcal{I}_h u\| = \mathcal{O}(h^2)$. We have that

$$\|u - \widetilde{u}_h\| + h\|\nabla[u - \widetilde{u}_h]\| \leq c_{\mathcal{I}} h^2 \|D^2 u\|.$$

With the continuity properties of the trace operator we deduce that

$$\begin{aligned}
&J_m(\widetilde{u}_h) - J_m(u) \\
&\leq \big(\nabla[\widetilde{u}_h + u], \nabla[\widetilde{u}_h - u]\big) + \frac{1}{m}\big(\|\widetilde{u}_h\|_{L^1(\partial\Omega)} + \|u\|_{L^1(\partial\Omega)}\big)\|\widetilde{u}_h - u\|_{L^1(\partial\Omega)} \\
&\leq ch\|u\|^2_{H^2(\Omega)},
\end{aligned}$$

which implies the first estimate.
(ii) Noting that $0 \leq |a|_\varepsilon - |a| \leq \varepsilon$ it follows that

$$\begin{aligned}
J_{m,\varepsilon}(u_h) - J_m(u_h) &= \frac{1}{m}\big(\|u_h\|_{L^1_\varepsilon(\partial\Omega)} + \|u_h\|_{L^1(\partial\Omega)}\big)\big(\|u_h\|_{L^1_\varepsilon(\partial\Omega)} - \|u_h\|_{L^1(\partial\Omega)}\big) \\
&\leq c(\|u_h\|_{H^1(\Omega)} + 1)\varepsilon.
\end{aligned}$$

We further note that we have

$$\int_{\partial\Omega} \big||u_h|_\varepsilon - \mathcal{I}_h|u_h|_\varepsilon\big| \, \mathrm{d}s \leq ch\|\nabla|u_h|_\varepsilon\|_{L^2(\partial\Omega)} \leq ch\|\nabla u_h\|_{L^2(\partial\Omega)}.$$

Using that for elementwise polynomial functions $\phi_h \in L^\infty(\Omega)$ we have

$$\|\phi_h\|_{L^2(\partial\Omega)} \leq ch^{-1/2}\|\phi_h\|_{L^2(\Omega)}$$

implies that

$$\begin{aligned}\big|J_{m,\varepsilon,h}(u_h) - J_{m,\varepsilon}(u_h)\big| &\\ &= \frac{1}{m}\big(\|u_h\|_{L^1_{\varepsilon,h}(\partial\Omega)} + \|u_h\|_{L^1_\varepsilon(\partial\Omega)}\big)\big|\|u_h\|_{L^1_{\varepsilon,h}(\partial\Omega)} - \|u_h\|_{L^1_\varepsilon(\partial\Omega)}\big| \\ &\le c\big(\|\nabla u_h\| + 1\big)h^{1/2}\|\nabla u_h\|,\end{aligned}$$

which proves the second estimate. □

The estimates of the proposition imply the Γ-convergence of the functionals $J_{m,\varepsilon,h}$ to J_m as $(\varepsilon, h) \to 0$. We formally extend the discrete functionals $J_{m,\varepsilon,h}$ by the value $+\infty$ in $H^1(\Omega) \setminus \mathcal{S}^1(\mathcal{T}_h)$. Note that the functional J_m is continuous, convex, and coercive on $H^1(\Omega)$.

Corollary 4.2. *The functionals $J_{m,\varepsilon,h}$ converge to J_m as $(\varepsilon, h) \to 0$ in the sense of Γ-convergence with respect to weak convergence in $H^1(\Omega)$.*

Proof. (i) Let $(u_h)_{h>0}$ be a sequence of finite element functions with $u_h \rightharpoonup u$ in $H^1(\Omega)$. The weak lower semicontinuity of J_m yields that

$$J_m(u) \le \liminf_{h\to 0} J_m(u_h).$$

Since by the second estimate of Proposition 4.1 we have

$$J_{m,\varepsilon,h}(u_h) - J_m(u_h) \to 0$$

as $(\varepsilon, h) \to 0$, we deduce that

$$J_m(u) \le \liminf_{h\to 0} J_{m,\varepsilon,h}(u_h).$$

(ii) Let $u \in H^1(\Omega)$ and $\delta > 0$. By continuity of J_m there exists $h_0 > 0$ such

$$|J_m(u) - J_m(u_h)| \le \delta/2$$

for all $u_h \in \mathcal{S}^1(\mathcal{T}_h)$ with $\|u - u_h\|_{H^1(\Omega)} \le h_0$. By Proposition 4.1 we have

$$|J_m(u_h) - J_{m,\varepsilon,h}(u_h)| \le \delta/2$$

for (ε, h) sufficiently small. By density of the spaces $\mathcal{S}^1(\mathcal{T}_h)$ in $H^1(\Omega)$ we may thus select a sequence $(u_h)_{h>0}$ with $u_h \to u$ in $H^1(\Omega)$ and

$$J_{m,\varepsilon,h}(u_h) \to J_m(u)$$

as $(\varepsilon, h) \to 0$. □

5. Numerical experiments

We illustrate the efficiency of the proposed numerical method and identify features of optimal insulating layers via several examples.

Example 5.1 (Unit disk)**.** *Let $d = 2$, $\Omega = B_1(0)$, and $m = 0.4$.*

The Neumann and Dirichlet eigenvalues for the Laplace operator on the unit disk coincide with certain squares of roots of Bessel functions and are given by

$$\lambda_D \approx 5.8503, \quad \lambda_N \approx 3.3979.$$

We initialized Algorithm 3.1 with random functions on approximate triangulations of $\Omega = B_1(0)$. Table 1 displays the number of nodes and triangles in $\mathcal{T}_h$, the number of iterations K needed to satisfy the stopping criterion

$$\|d_t u_h^K\|_* \leq \varepsilon_{\text{stop}},$$

and the approximations

$$\lambda_{m,\varepsilon,h} = \frac{J_{m,\varepsilon,h}(u_h^K)}{\|u_h^K\|^2}$$

with the final iterate u_h^K. We used a lumped L^2 inner product to define the evolution metric $(\cdot,\cdot)_*$. The regularization parameter, the step size, and the stopping criterion were defined via

$$\varepsilon = h/10, \quad \tau = 1, \quad \varepsilon_{\text{stop}} = h/10.$$

Plots of the numerical solutions in Example 5.1 on triangulations with 1024 and 4096 triangles are shown in Figure 3. The break of symmetry becomes appearant and is stable in the sense that it does not change with the discretization parameters. From the numbers in Table 1 we see that the iteration numbers grow slower than linearly with the inverse of the mesh size and that the approximations of λ_m converge without a significant preasymptotic range. For a comparison we computed the eigenvalue of the operator $\mathcal{A}_\ell$ with constant function $\ell(s) = m/|\partial\Omega|$ and obtained the value $\lambda_{m,\ell} \approx 5.095$ for $m = 0.4$, i.e., the nonuniform distribution of insulating material reduces the eigenvalue by approximately 0.5%.

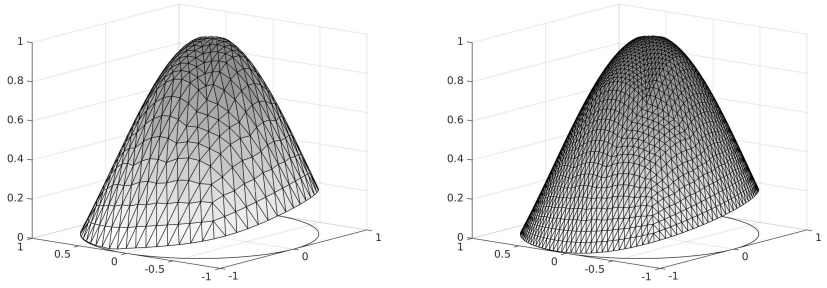

FIGURE 3. Eigenfunctions for different triangulations in Example 5.1.

Example 5.2 (Unit square)**.** *Let $d = 2$, $\Omega = (0,1)^2$, and $m = 0.1$.*

On the unit square we have

$$\lambda_D = 2\pi^2, \quad \lambda_N = \pi^2,$$

h	$\#\mathcal{N}_h$	$\#\mathcal{T}_h$	K	$\lambda_{m,\varepsilon,h}$
2^{-1}	13	16	9	4.938 371
2^{-2}	41	64	9	5.018 139
2^{-3}	145	256	8	5.063 251
2^{-4}	545	1024	16	5.070 124
2^{-5}	2113	4096	70	5.071 488
2^{-6}	8321	16384	107	5.071 643
2^{-7}	33025	65536	161	5.071 725
2^{-8}	131585	262144	224	5.071 721
2^{-9}	525313	1048576	260	5.071 709

TABLE 1. Iteration numbers and discrete eigenvalues in Example 5.1.

and the qualitative properties of optimal insulations differ significantly from those for the unit disk. Figure 4 displays numerical solutions on triangulations of $\Omega = (0,1)^2$ with 289 and 1089 triangles in Example 5.2. We observe that the computed solutions reflect the symmetry properties of the domain but also correspond to a nonuniform distribution of insulating material. In this experiment significantly smaller iteration numbers are observed which appear to be related to the symmetry and corresponding uniqueness properties of solutions. The fact that the computed eigenvalues shown in Table 2 may increase for enlarged spaces is due to the use of the mesh-dependent regularization and quadrature.

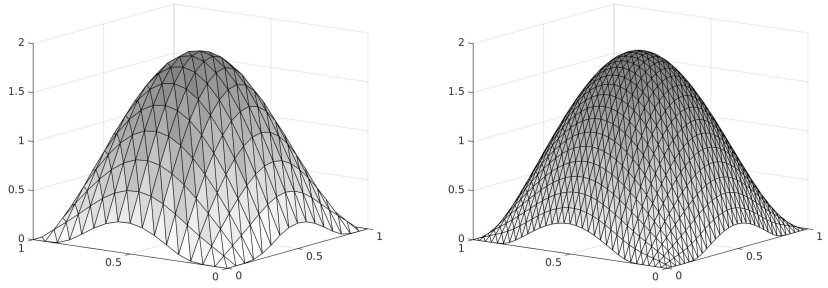

FIGURE 4. Eigenfunctions for different triangulations in Example 5.2.

Example 5.3 (Unit ball)**.** *Let $d = 3$, $\Omega = B_1(0)$, and $m = 5.0$.*

The effect of a nonuniform insulating layer is slightly stronger in three-dimensional situations. For the setting of Example 5.3 and two different triangulations we obtained the distributions shown in Figure 5. As in two space dimensions the insulation leaves a connected gap which is here approximately circular. The thickness continuously increases to a maximal value that is attained at a point on the boundary which is opposite to the gap of the insulation. Note that the position of the gap is arbitrary and depends on the initial data and the discretization parameters. For a uniform distribution of the insulation material we obtain the Robin eigenvalue

h	$\#\mathcal{N}_h$	$\#\mathcal{T}_h$	K	$\lambda_{m,\varepsilon,h}$
2^{-1}	9	8	6	14.648 110
2^{-2}	25	32	6	16.734 246
2^{-3}	81	128	7	17.060 456
2^{-4}	289	512	9	17.090 222
2^{-5}	1089	2048	14	17.093 521
2^{-6}	4225	8192	13	17.094 441
2^{-7}	16641	32768	16	17.091 990
2^{-8}	66049	131072	21	17.090 093
2^{-9}	263169	524288	25	17.089 322

TABLE 2. Iteration numbers and discrete eigenvalues in Example 5.2.

$\lambda_R = 4.7424$ so that the nonuniform distribution reduces the slightly larger limiting value of Table 3 by approximately 1%.

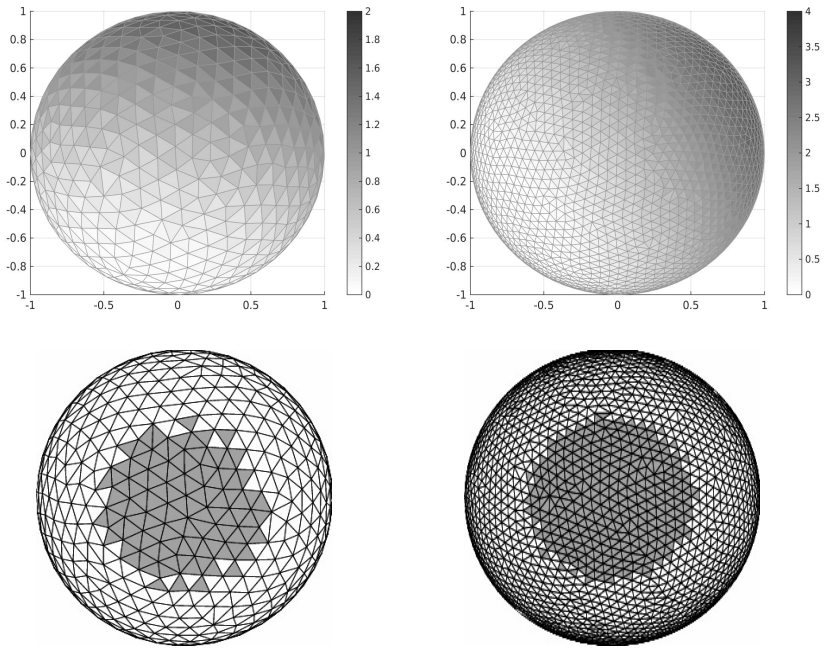

FIGURE 5. Eigenfunctions for different triangulations (top) and approximate indicator functions of the insulation gaps after rotation (bottom) in Example 5.3.

6. SHAPE VARIATIONS

6.1. **Shape optimization.** The insulation properties of a conducting body can further be improved by modifying its shape keeping its volume fixed. Taking perturbations of the domain gives rise to a shape derivative of the

h	$\#\mathcal{N}_h$	$\#\mathcal{T}_h$	K	$\lambda_{m,\varepsilon,h}$
2^{-1}	33	87	9	4.587 743
2^{-2}	257	1069	11	4.696 848
2^{-3}	2205	11162	45	4.693 606
2^{-4}	17461	96384	133	4.692 364
2^{-5}	138745	796358	161	4.692 733

TABLE 3. Iteration numbers and discrete eigenvalues in Example 5.3.

eigenvalue λ_m regarded as a function of the domain Ω, i.e., for a vector field $w : \Omega \to \mathbb{R}^d$ and a number $s \in \mathbb{R}$ we consider the perturbed domain $(\mathrm{id} + sw)(\Omega)$ and define

$$\delta\lambda_m(\Omega)[w] = \lim_{s\to 0} \frac{\lambda_m\big((\mathrm{id} + sw)(\Omega)\big) - \lambda_m\big(\Omega\big)}{s}.$$

It follows from, e.g., [HP05, BBN17], that with the outer unit normal n on $\partial\Omega$ we have

$$\delta\lambda_m(\Omega)[w] = \int_{\partial\Omega} j_m(u) w \cdot n \,\mathrm{d}s,$$

where $j_m(u)$ is for a sufficiently regular, nonnegative eigenfunction $u \in H^1(\Omega)$ corresponding λ_m and the mean curvature H on $\partial\Omega$, normalized so that $H = d - 1$ for the unit sphere, given by

$$j_m(u) = |\nabla u|^2 - 2|\partial_n u|^2 - \lambda_m u^2 + \frac{2}{m}\|u\|_{L^1(\partial\Omega)} Hu.$$

To preserve the volume of Ω we restrict to divergence-free vector fields and compute a representative $v = \nabla_{\mathrm{St}}\lambda_m(\Omega) \in H^1(\Omega;\mathbb{R}^d)$ of $\delta\lambda_m(\Omega)$ via the Stokes problem

$$\begin{cases} (v, w) + (\nabla v, \nabla w) + (p, \operatorname{div} w) = \delta\lambda_m(\Omega)[w], \\ (q, \operatorname{div} v) = 0, \end{cases}$$

for all $w \in H^1(\Omega;\mathbb{R}^d)$ and $q \in L^2(\Omega)$. Since $\delta\lambda_m(\Omega)[w]$ only depends on the normal component $w \cdot n$ on $\partial\Omega$ it follows that the tangential component of the solution $v \in H^1(\Omega;\mathbb{R}^d)$ vanishes. To optimize λ_m with respect to shape relative to a reference domain $\Omega \subset \mathbb{R}^d$ we evolve the domain by the negative shape gradient, i.e., beginning with $\Omega_0 = \Omega$ we define a sequence of domains $(\Omega_k)_{k=0,1,\dots}$ via

$$\Omega_{k+1} = (\mathrm{id} + \tau_k v_k)(\Omega_k), \quad v^k = -\nabla_{\mathrm{St}}\lambda_m(\Omega_k),$$

with positive step sizes $\tau_k > 0$. Starting from a maximal initial step size $\tau_{\max}$, we decreased the step size τ_k in the k-th step of the gradient descent until a relative decrease of the objective below $0 < \theta < 1$ is achieved. The new step size is then defined by $\tau_{k+1} = \min\{\tau_{\max}, 2\tau_k\}$; we stop the iteration if $\tau_{k+1} \le \varepsilon'_{\mathrm{stop}}$.

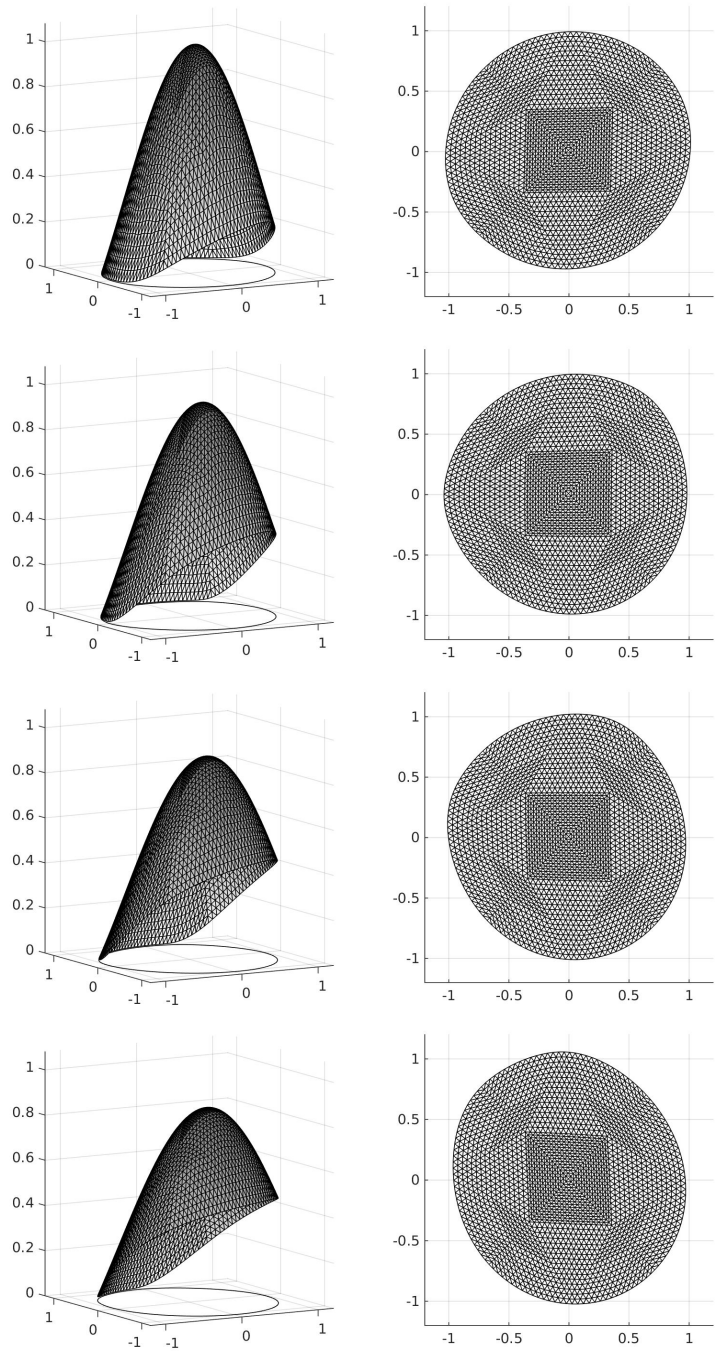

FIGURE 6. Eigenfunctions u_m and corresponding optimized two-dimensional shapes Ω^* obtained from the unit disk $\Omega = B_1(0)$ with $m = 0.4$, 0.9, 1.4, 1.9 (top to bottom).

6.2. **Optimization from the unit disk.** Starting from the unit disk and using different values m for the available insulation mass we carried out a shape gradient descent iteration using a discretization of the Stokes problem with a nonconforming Crouzeix–Raviart method. The numerical solutions v_h^k were projected onto conforming $P1$ finite element vector fields before the triangulation of the current domain was deformed. Figure 6 shows the computed nearly stationary shapes for $m = 0.4, 0.9, 1.4, 1.9$ along with eigenfunctions u_m. We see that the boundary is flatter along the parts which are not insulated and that the domains are convex with one axis of symmetry. The reduction of the eigenvalues via shape optimization is rather small as is documented in Table 4 in which the eigenvalues $\lambda_R^{\rm uni}(\Omega)$, $\lambda_{m,h}(\Omega)$, and $\lambda_{m,h}(\Omega^*)$ for the uniform and nonuniform insulation of the unit disk and the optimized domains Ω^*, respectively, are displayed.

m	0.4	0.9	1.4	1.9
$\lambda_R^{\rm uni}(\Omega)$	5.0951	4.3803	3.8085	3.3519
$\lambda_{m,h}(\Omega)$	5.0714	4.3383	3.7819	3.3503
$\lambda_{m,h}(\Omega^*)$	5.0664	4.3296	3.7718	3.3378

TABLE 4. Decrease of the nonlinear eigenvalues via shape optimization for different total masses and comparison to uniform insulations on the unit disk $\Omega = B_1(0)$.

6.3. **Three-dimensional rotational shapes.** The optimization of $\lambda_m(\Omega)$ among domains $\Omega \subset \mathbb{R}^d$ is ill-posed when $d \geq 3$ as explained in the introduction. The same phenomenon is obtained by taking $\Omega = B_{r_1} \cup B_{r_2}$ the union of two disjoint balls with radii r_1 and r_2 and

$$u = \begin{cases} 1 & \text{on } B_{r_1} \\ 0 & \text{on } B_{r_2} \end{cases}$$

which gives

$$\lambda_m(\Omega) \leq \frac{\frac{1}{m}(|\partial B_{r_1}|)^2}{|B_{r_1}|} = \frac{d^2\omega_d}{m} r_1^{d-2} \,.$$

Again, $\lambda_m(\Omega)$ can be made arbitrarily small, keeping the measure of Ω fixed and letting $r_1 \to 0$.

Instabilities in numerical experiments confirm the general ill-posedness in the three-dimensional setting. It is expected that optimal shapes exist among convex bodies of fixed volume and we therefore carried out a one-dimensional optimization among ellipsoids

$$\Omega_a = \text{ellipsoid with radii } (a, r_a, r_a).$$

The radii r_a are chosen such that $|\Omega_a| = c_0$. Letting $c_0 = |B_1(0)|$ and $m = 5.0$ be the volume of the unit ball and total mass we plotted in Figure 7 the values $\lambda_m(\Omega_a)$ as a function of $a \in [1, 1.5]$. For numerical efficiency

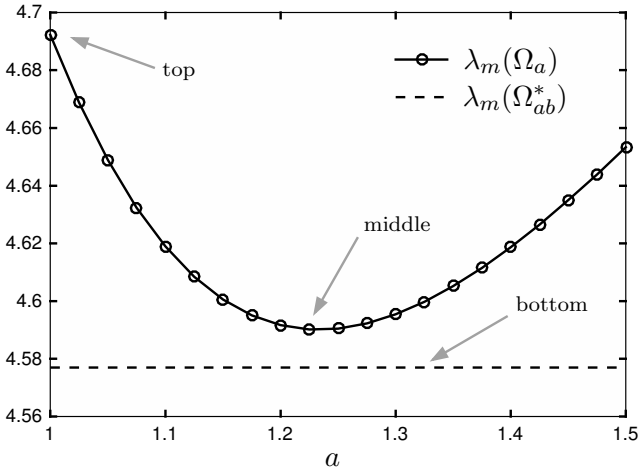

FIGURE 7. Eigenvalues $\lambda_m(\Omega_a)$ for different symmetric ellipsoids and optimal assembled half-ellipsoids $\lambda_m(\Omega^*_{ab})$ and references to corresponding shapes shown in Figure 8.

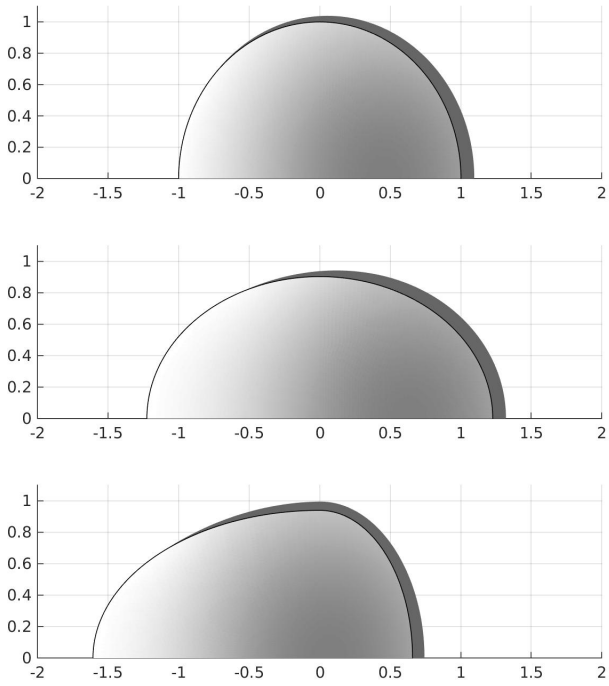

FIGURE 8. Profile, eigenfunction (gray shading), and boundary film (scaled by $\varepsilon = 1/10$) for the unit ball Ω_1 (top), the optimal ellipsoid Ω_a with $a = 1.225$ (middle), and the optimal assembled half-ellipsoids Ω^*_{ab} with $a = 1.607$ and $b = 0.657$ (bottom).

we exploited the rotational symmetry of the domains and discretized the dimensionally reduced setting. We obtain an optimal value for the radius $a \approx 1.225$. The profile of this ellipsoid and a corresponding eigenfunction u_m are displayed in the top and middle plot of Figure 8. We further optimized the eigenvalue within a larger class of rotational bodies defined as assembled half-ellipsoids, i.e., by considering

$$\overline{\Omega}_{ab} = \big(\overline{\Omega}_a \cap \{x_1 \le 0\}\big) \cup \big(\overline{\Omega}_b \cap \{x_1 \ge 0\}\big),$$

and adjusting the radii $r_a = r_b$ such that $|\Omega_{ab}| = c_0$. Optimizing among the radii (a, b) we find the optimal shape shown in the bottom plot of Figure 8. The corresponding discrete eigenfunction is visualized by the gray shading and suggests a gap in the insulation at the pointed and a thicker insulation on the blunt end on the surface of the egg-like optimal domain.

Acknowledgments: S.B. acknowledges hospitality of the Hausdorff Research Institute for Mathematics within the trimester program *Multiscale Problems: Algorithms, Numerical Analysis and Computation* and support by the DFG via the priority program *Non-smooth and Complementarity-based Distributed Parameter Systems: Simulation and Hierarchical Optimization* (SPP 1962). G.B. is member of the Gruppo Nazionale per l'Analisi Matematica, la Probabilità e le loro Applicazioni (GNAMPA) of the Istituto Nazionale di Alta Matematica (INdAM); his work is part of the project 2015PA5MP7 *"Calcolo delle Variazioni"* funded by the Italian Ministry of Research and University.

References

[AB86] Emilio Acerbi and Giuseppe Buttazzo, *Reinforcement problems in the calculus of variations*, Ann. Inst. H. Poincaré Anal. Non Linéaire **3** (1986), no. 4, 273–284.

[BBN17] Dorin Bucur, Giuseppe Buttazzo, and Carlo Nitsch, *Symmetry breaking for a problem in optimal insulation*, J. Math. Pures Appl. (9) **107** (2017), no. 4, 451–463.

[BCF80] Haïm Brézis, Luis A. Caffarelli, and Avner Friedman, *Reinforcement problems for elliptic equations and variational inequalities*, Ann. Mat. Pura Appl. (4) **123** (1980), 219–246.

[BDN17] Sören Bartels, Lars Diening, and Ricardo H. Nochetto, *Stable discretization of singular flows*, in preparation, 2017.

[CKU99] S. J. Cox, B. Kawohl, and P. X. Uhlig, *On the optimal insulation of conductors*, J. Optim. Theory Appl. **100** (1999), no. 2, 253–263.

[Dzi99] Gerd Dziuk, *Numerical schemes for the mean curvature flow of graphs*, Variations of domain and free-boundary problems in solid mechanics (Paris, 1997), Solid Mech. Appl., vol. 66, Kluwer Acad. Publ., Dordrecht, 1999, pp. 63–70.

[Fri80] Avner Friedman, *Reinforcement of the principal eigenvalue of an elliptic operator*, Arch. Rational Mech. Anal. **73** (1980), no. 1, 1–17.

[HP05] Antoine Henrot and Michel Pierre, *Variation et optimisation de formes*, Mathématiques & Applications (Berlin) [Mathematics & Applications], vol. 48, Springer, Berlin, 2005, Une analyse géométrique. [A geometric analysis].

Sören Bartels: Abteilung für Angewandte Mathematik, Universität Freiburg
Hermann-Herder-Str. 10, 79104 Freiburg im Breisgau - GERMANY

bartels@mathematik.uni-freiburg.de
https://aam.uni-freiburg.de/bartels

Giuseppe Buttazzo: Dipartimento di Matematica, Università di Pisa
Largo B. Pontecorvo 5, 56127 Pisa - ITALY
buttazzo@dm.unipi.it
http://www.dm.unipi.it/pages/buttazzo/